
AFRL-AFOSR-VA-TR-2019-0367

# THE COMPUTATIONAL DESIGN OF OLIGOMERS FOR USE IN HIGH CONSTRAST BLACK ELECTROCHROMIC POLYMERS

**Aimee Tomlinson**
**University Of North Georgia**

**12/12/2019**
**Final Report**



Air Force Research Laboratory
AF Office Of Scientific Research (AFOSR)/ RTB2
Arlington, Virginia 22203
Air Force Materiel Command

DISTRIBUTION A: Distribution approved for public release.

# REPORT DOCUMENTATION PAGE

*Form Approved*
*OMB No. 0704-0188*



| 1. REPORT DATE *(DD-MM-YYYY)* | 2. REPORT TYPE | 3. DATES COVERED *(From - To)* |
|---|---|---|
| 12-12-2019 | Final Performance | 01 Nov 2017 to 31 Oct 2019 |

**4. TITLE AND SUBTITLE**
THE COMPUTATIONAL DESIGN OF OLIGOMERS FOR USE IN HIGH CONSTRAST BLACK ELECTROCHROMIC POLYMERS

**5a. CONTRACT NUMBER**

**5b. GRANT NUMBER**
FA9550-18-1-0034

**5c. PROGRAM ELEMENT NUMBER**
61102F

**6. AUTHOR(S)**
Aimee Tomlinson

**5d. PROJECT NUMBER**

**5e. TASK NUMBER**

**5f. WORK UNIT NUMBER**

**7. PERFORMING ORGANIZATION NAME(S) AND ADDRESS(ES)**
University Of North Georgia
82 COLLEGE CIR
DAHLONEGA, GA 30597 US

**8. PERFORMING ORGANIZATION REPORT NUMBER**

**9. SPONSORING/MONITORING AGENCY NAME(S) AND ADDRESS(ES)**
AF Office of Scientific Research
875 N. Randolph St. Room 3112
Arlington, VA 22203

**10. SPONSOR/MONITOR'S ACRONYM(S)**
AFRL/AFOSR RTB2

**11. SPONSOR/MONITOR'S REPORT NUMBER(S)**
AFRL-AFOSR-VA-TR-2019-0367

**12. DISTRIBUTION/AVAILABILITY STATEMENT**
A DISTRIBUTION UNLIMITED: PB Public Release

**13. SUPPLEMENTARY NOTES**

**14. ABSTRACT**
During this grant period, we have published four manuscripts one purely theoretical and three which were a collaboration with the Reynolds group. One of our biggest accomplishments was the development of the first reported colorimetric model at the DFT level. We were also able to use this model in order to identify the aryl group combinations which were likely responsible for the peaks in the yellow-black polymer discussed in the previously manuscript with Reynolds. Additionally, within this time frame we have performed hundreds of DFT/TDDFT computations on a variety of oligomers in effort to gain further insight into structure property relationships which provide us with design rules for future oligomer and polymer systems. In one of these studies we found that meta and para substituted benzene rings coupled with alkyl or thioalkyl side-chains provide the best ring strain stabilization which is necessary for anodically coloring electrochromes (ACEs). As a consequence of this study, we worked with the Reynolds group and identified a set of high gap ACEs where the electron-donating or withdrawing nature of the substituent resulted in a color change for the radical cation. Additionally, we published a paper with the Reynolds group detailing an all donor set of terpolymers which may be combined together to generate a color palette which covers a significant amount of color space while maintaining low oxidation potentials, high contrast, and long-lasting optical memory. Finally, one of our last studies involved a symmetry approach to the number of allowable excited states and thereby the color.

**15. SUBJECT TERMS**
Electrochromic Polymers, CMY Comination Chromophores, Computational Chemstry, DFT and TD-DFT Computation

| 16. SECURITY CLASSIFICATION OF: | | | 17. LIMITATION OF ABSTRACT | 18. NUMBER OF |
|---|---|---|---|---|
| | | | | |

| a. REPORT | b. ABSTRACT | c. THIS PAGE | | PAGES | 19a. NAME OF RESPONSIBLE PERSON |
|---|---|---|---|---|---|
| Unclassified | Unclassified | Unclassified | UU | | CASTER, KENNETH |
| | | | | | 19b. TELEPHONE NUMBER *(Include area code)* 703-588-8487 |

Final Report

For

AFOSR Grant

17RT0234
(FA9550-18-1-0034)

# A COMPUTATIONAL DESIGN OF OLIGOMERS FOR USE IN HIGH CONSTRAST BLACK ELECTROCHROMIC POLYMERS

Reporting Period:

November 1, 2017 – October 31, 2019

*Program Manager:*

Kenneth Caster
Air Force Office of Scientific Research

*Principal Investigator:*

Aimée L. Tomlinson
Department of Chemistry & Biochemistry
University of North Georgia
82 College Circle Dahlonega, GA 30597

706-867-3232 (ph)
412-760-2268(cell)
Email: aimee.tomlinson@ung.edu

## I. Statement of Objectives

The goal of this proposed effort is to use theoretical calculations to identify electrochromic oligomeric structures change from highly transmissive to high constrast black or from black to transmissive as they either oxidized or reduced. This work will be carried out as an active collaboration with the synthetic effort of the Reynolds group at Georgia Tech in the design of pure, blends, or copolymers for switching electrochromic materials. We will form a tight feedback loop between our group and the Reynolds group, such that the computational effort will narrow down the promising oligomers which will then be synthesized and characterized, then fed back to computation for continuous benchmarking. We will utilize a DFT/TDDFT set of treatments to identify the structures which have the most promise to generate neutral oligomers with little to no absorption in the visible thereby guaranteeing a nearly 100% transmissive material while the oxidized state appears black. Our approach will be to start with known materials the Reynolds group has already examined and apply modular changes to both the backbone as well as the side-chains.

## II. Accomplishment Overview

During this grant period, we have published four manuscripts one purely theoretical and three which were a collaboration with the Reynolds group. One of our biggest accomplishments was the development of the first reported colorimetric model at the DFT level. We were also able to use this model in order to identify the aryl group combinations which were likely responsible for the peaks in the yellow-black polymer discussed in the previously manuscript with Reynolds. Additionally, within this time frame we have performed hundreds of DFT/TDDFT computations on a variety of oligomers in effort to gain further insight into structure property relationships which provide us with design rules for future oligomer and polymer systems. In one of these studies we found that meta and para substituted benzene rings coupled with alkyl or thioalkyl side-chains provide the best ring strain stabilization which is necessary for anodically coloring electrochromes (ACEs). As a consequence of this study, we worked with the Reynolds group and identified a set of high gap ACEs where the electron-donating or –withdrawing nature of the substituent resulted in a color change for the radical cation. Additionally, we published a paper with the Reynolds group detailing an all donor set of terpolymers which may be combined together to generate a color palette which covers a significant amount of color space while maintaining low oxidation potentials, high contrast, and long-lasting optical memory. Finally, one of our last studies involved a symmetry approach to the number of allowable excited states and thereby the color.

## III. Specific Task Accomplishments

### *III.1 Our Model*

*Wheeler, D., Rainwater, L., Green, A., Tomlinson, A., "Modeling electrochromic poly-dioxythiophene-containing materials through TDDFT", Phys. Chem. Chem. Phys.,* ***2017****, 19, 20251-20258. doi.org/10.1039/c7cp04130f.*

III.1A *Computational Methodology:* All computations were performed using Gaussian 09.[1] We first tested hybrid functional/basis set combinations against the available experimental results[2] to identify the optimum combination. Additionally, the polarizable conductor calculation model (CPCM)[3] was utilized to emulate a dielectric environment for the solvent dichloromethane (DCM). After benchmarking we found that the mPW1PBE[4]/cc-PVDZ[5] provided the best correlation to the experimental data. Our process began with structural optimization of each neutral oligomer at the DFT level. Next, the first thirteen excited states using perturbative TD-DFT were performed to generate the UV-Vis spectra. With all experimental data being collected in solid-state, it was assumed that the structural modifications each system would undergo upon oxidation would be minimal. Therefore, the polaron and bipolaron data was produced using the optimized neutral geometries with charge inclusion.[6]

III.1B *Determination of Oligomer Size Needed to Model Polymer*: The first objective was to determine what size oligomer was required for modeling. Once acquired, neutral electronic transition data for the color

standards were determined and oxidized state calculations were performed. The normalized simulated UV-Vis spectra of various CMY oligomers compared to the normalized experimental spectra are shown in **Figure 1**. To no surprise, it is found that as the conjugation of each oligomeric calculation increases, the absorbance undergoes a bathochromic shift. It was determined that the simulated spectrum has comparable peak maxima with experimental data upon inclusion of a total of six heterocycles for each color. For cyan, two experimental maxima are observed. The first experimental maxima at 681 nm correlates to the simulated maxima at 695 nm, producing an absolute difference of 14 nm. The second maxima occurs at 405 nm, containing only a 3 nm difference relative to the experimental maxima (408 nm). In the case of magenta, experimental peaks are found at 594 nm and 550 nm producing an absolute difference of 1 nm in comparison to the model (549 nm). Finally for yellow, the experimental data contains only one observed peak at 447 nm leading to an absolute difference of 1 nm in correlation to 446 nm peak from the model.

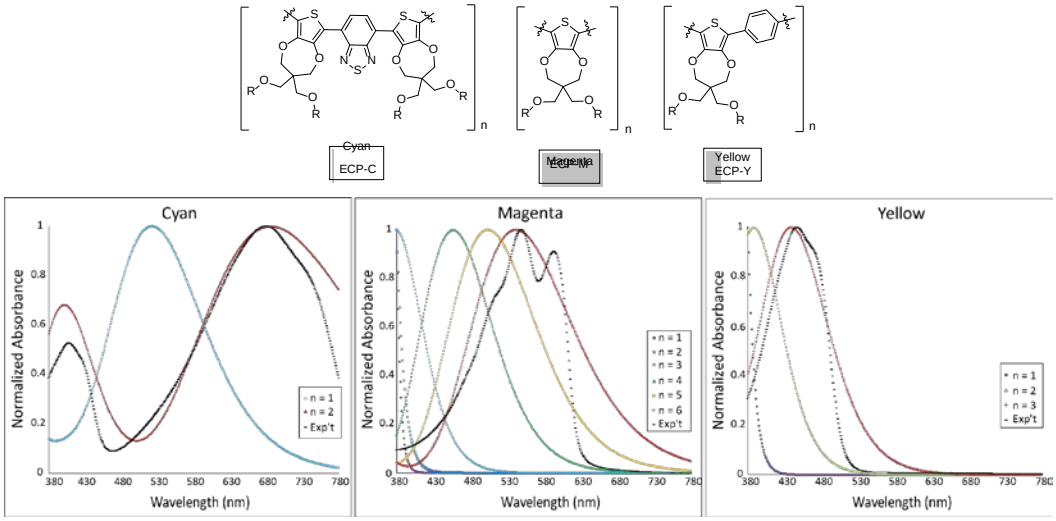


| | | | | | |
|---|---|---|---|---|---|
| $\lambda_{exp't}$ | 681 nm | $\lambda_{exp't}$ | 594, 550 nm | $\lambda_{exp't}$ | 447 nm |
| $\lambda_{DFT}$ | 695 nm | $\lambda_{DFT}$ | 549 nm | $\lambda_{DFT}$ | 446 nm |
| *Abs. Diff.* | 14 nm | *Abs. Diff.* | 1 nm | *Abs. Diff.* | 1 nm |

**Figure 1:** Determination of the oligomer size which best reproduces Reynolds' group UV-Vis data.

III.1C *Detailed Transition and FMO Study for Neutral Species:* To gain a better understanding of the excited states, a detailed analysis of the transitions that led to these states was performed. Excited states with oscillator strengths ($f$) of 0.20 and higher were calculated for all three chromophores that were evaluated. In the case of cyan, the first excited state ($\lambda$ = 695 nm) with an $f$ = 1.51 possesses two transitions with H→L (97.5%) being the dominant. The second cyan excited state ($\lambda$ = 405 nm) is found to contain an $f$ = 0.84 and is formed primarily by the H-2→L transition (77.4%). A close examination of the frontier molecular orbitals (FMOs) shown in Figure 3 indicates that the electron density is delocalized throughout the pi-system for both the H-1 and H levels. Upon excitation, the electron density shifts toward the electron withdrawing benzothiadiazole (BTD) heterocycles in L and L+1. These donor-acceptor interactions have been investigated and been shown to decrease the band gap of the materials by lowering the LUMO and raising the HOMO.[6-7] Similar studies were performed for both the magenta and yellow polymers.

III.1D *Oligomer Color Study*

Neutral Oligomers: In order to translate the predicted UV-Vis spectra into a perceivable color, L*, a*, and b* coordinates were determined using a Matlab script provided by the Reynolds group.[59] These coordinates can be thought of as a hemisphere centered on a 3-dimensional graph. Two axes, a* and b*, describe the amount of mixing and saturation between two colors which fall in a range from -100 to +100. The last axis, L*, indicates the brightness of these mixed colors in a range of 0 to 100.[60] A L* value of 100

is indicative of white and 0 is black. For the a* scale, -100 correlates to green while +100 is indicative of red. For b*, the negative limit corresponds to blue while the positive to yellow. A comparison between the experimental and DFT color coordinate data is summarized in **Table 1A**. Both sets of numbers as well as the color swatches indicate a good correlation between the two sets of data. It can be seen in the cyan coordinates that there is excellent L* correspondence between experiment and theory, but a slight green shift in the a* value and yellow shift in the b*. The reason this occurs is explained through a close examination of the absorption minimum. In the simulated spectrum, the observed minimum appears at approximately 500 nm, which lies closer to the green region of the visible spectrum. However, the experimental minimum is found to occur closer to 450 nm, which is visibly more blue. For magenta, a green shift for the a* value and a blue shift for the b* coordinate produces an indigo color. Finally, the yellow polymer had a significant red shift in the a* value and slight blue shift in the b* coordinate, leading to an orange-gold color. The error in these modelled colorimetric values for magenta and yellow is again attributed to a Gaussian curve fit which produced peak broadening.[1] This broadening caused an excess absorbance of lower energy light for each simulation. Another contribution comes from the fact that each computation only included one oligomer, eliminating the effects of intermolecular interactions such as π-π stacking.

**Table 1A:** Neutral color data in which the experimental and computational measurements are shown.

| | Cyan | | Magenta | | Yellow | |
|---|---|---|---|---|---|---|
| | *Exp't* | *DFT* | *Exp't* | *DFT* | *Exp't* | *DFT* |
| L* | 71 | 74 | 53 | 46 | 96 | 86 |
| a* | -34 | -47 | 51 | 43 | -7 | 17 |
| b* | -21 | -6 | -41 | -58 | 84 | 72 |
| R | 0 | 0 | 177 | 123 | 255 | 255 |
| G | 192 | 205 | 92 | 85 | 243 | 200 |
| B | 211 | 191 | 198 | 207 | 0 | 71 |

**Table 1B:** Bipolaron color data in which the experimental and computational measurements are shown.

| | Cyan | | Magenta | | Yellow | |
|---|---|---|---|---|---|---|
| | *Exp't* | *DFT* | *Exp't* | *DFT* | *Exp't* | *DFT* |
| L* | 86 | 99 | 91 | 99 | 89 | 99 |
| a* | -3 | -2 | -2 | -3 | 1 | -2 |
| b* | -3 | -1 | -4 | -2 | 0 | -1 |
| R | 206 | 247 | 221 | 244 | 223 | 247 |
| G | 217 | 253 | 231 | 254 | 220 | 253 |
| B | 221 | 254 | 237 | 255 | 221 | 254 |

Oxidized Oligomers: By translating spectral data into colorimetric coordinates, further insight between the relationship of transmissivity and spectroscopic features is shown in **Table 1B**. The computed L*a*b*/RGB values were nearly colorless and transparent whereas the experimental values retained blue and slightly grey hues. For all oligomers, the L* value from the DFT calculations is found to be 99, producing high transmissivity. When compared to experimental data, this value overstates the level of transparency each polymer would generate. This overstatement in transmissivity is again attributed to the Gaussian fit about the predicted excited states. A close examination of the experimental L* values indicated there is an increase in transmissivity going from cyan (86) to yellow (88) to magenta (91). The DFT a* and b* values only deviate from experiment by ±2, indicating excellent color correlation. Overall, oxidized colorimetric data over-expressed the transmissivity of these material, but the DFT simulated spectra did provide accurate color.

### *III.2 Application of DFT/TDDFT Model on Anodically Coloring Yellow-Black Polymer*

*Christiansen, D., Wheeler, D., Tomlinson, A., Reynolds, J. "Electrochromism of alkylene-linked discrete chromophore polymers with broad radical cation light absorption", Polymer Chemistry, **2018**, **9**, 3055-3066, DOI: 10.1039/c8py00385h.*

*III.2A Anodically Coloring Materials*: Here, we explore anodic coloration as a methodology for designing electrochromic polymers where we avoid the NIR tailing observed in cathodically coloring ECPs as demonstrated in **Figure 2**. These materials are designed to have electron rich, conjugated chromophores of discrete length, which have wide optical gaps absorbing specifically in the UV in their neutral state with minimal tailing into the visible in the colorless state. This can be seen by the solid curve in **Figure 2**. Upon oxidation to the radical cation state, short conjugation lengths maintain a high-energy absorption relative to

fully conjugated polymer systems, moving the absorbance into the visible region (380-780 nm). This broad dual band absorbance is denoted by the dashed curve. In order to effectively design these materials as effective high contrast electrochromes, a fundamental understanding must be developed on how conjugation length, electron-rich character, and steric strain control the redox potential for switching to, and the absorption characteristics of, the radical cation state.

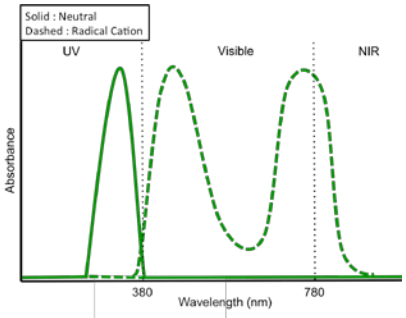


**Figure 2**: Spectra for ideal anodically coloring material with a UV absorbing neutral state and broadly absorbing radical cation state.

*III.2B Interring Strain Study:* The impact of interring strain between neutral and oxidized states was examined utilizing the first set of ter(heterocycle) systems shown in **Scheme 1**. Each chromophore contained terminal groups of methyl-capped 3,4-ethylenedioxythiophene (**E**) and a distinct middle heterocycle: either a branched alkyl ether functionalized 3,4-propylenedioxythiophene (**P**) or a 3,4-bis(2-ethylhexyloxy)thiophene (**A**). By changing the identity of the middle heterocycle, the proximity of the alkoxy-chains relative to the conjugated backbone varied as a function of distance, while the number of π-electrons in the chromophore remained unchanged. The degree of interring strain was determined by observing the changes in dihedral angles between the terminal and middle heterocycles in each chromophore.

The results of the structural data for these ter(heterocycles) from the optimized geometry are collated in **Table 2**. The rings were numbered in each chromophore, and the interring bond lengths, dihedral angles, and first excited state energies (TD-DFT HOMO-LUMO gap) were measured. Examining the dihedral angle measurements, it is clear that the proximity of the 2-ethylhexyl solubilizing groups affect the degree of conjugation as the HOMO-LUMO gap for **EAE** is 0.68 eV higher than **EPE**. Since the solubilizing chains are farther from the backbone of the chromophore in **EPE**, all three heterocycles remain in excellent conjugation with one another, independent of the charged state. However, for the neutral **EAE** chromophore, only two of the three heterocycles are found to be exceptionally planar (175.2°) while the third heterocycle remains orthogonal (91.5°). Upon oxidation, the **EAE** chromophore becomes increasingly planar, reducing the orthogonal character (178.8° and 164.4°). The oxidized chromophores exhibit more quinoidal character as the bond length between heterocycles decrease by ~0.03 Å.

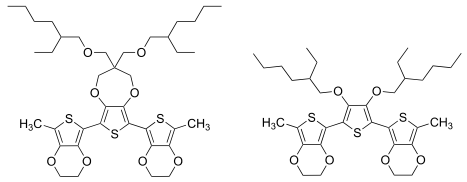


**Scheme 1.** Methyl-terminated ter(heterocycles) evaluated in the strain study.

**Table 2:** Structural data for all target oligomers in this study. The figure key shows how rings and dihedral angles are numbered and symbolized in the table.

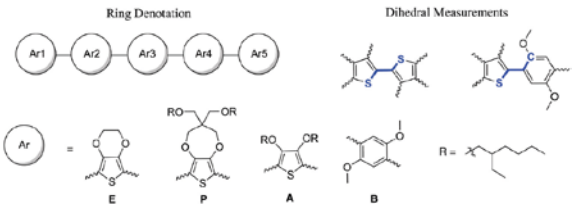


| | EPE | | EAE | | EAAE | | EABAE | |
|---|---|---|---|---|---|---|---|---|
| | Neutral | Polaron | Neutral | Polaron | Neutral | Polaron | Neutral | Polaron |
| Ar1-Ar2 (Å) | 1.44 | 1.41 | 1.46 | 1.41 | 1.44 | 1.41 | 1.46 | 1.41 |
| Ar2-Ar3 (Å) | 1.44 | 1.41 | 1.44 | 1.41 | 1.46 | 1.41 | 1.47 | 1.44 |
| Ar3-Ar4 (Å) | -- | -- | -- | -- | 1.45 | 1.41 | 1.47 | 1.44 |
| Ar4-Ar5 (Å) | -- | -- | -- | -- | -- | -- | 1.46 | 1.42 |
| Ar1-Ar2 dihedral | 177.2 | 178.1 | 91.5 | 164.4 | 179.2 | 179.7 | 86.8 | 167.3 |
| Ar2-Ar3 dihedral | 177.2 | 178.1 | 175.2 | 178.8 | 151.4 | 151.4 | 121.5 | 137.7 |
| Ar3-Ar4 dihedral | -- | -- | -- | -- | 174.8 | 179.7 | 125.6 | 132.5 |
| Ar4-Ar5 dihedral | -- | -- | -- | -- | -- | -- | 83.7 | 169.1 |

The structural models for the ter(heterocycles) are corroborated with the analysis of the calculated UV-Vis spectra as depicted in **Figure 3**. The absorption of **EPE** ($\lambda_{max}$ = 413 nm) occurs extensively throughout the visible due to a lack of interring strain, while the converse is observed for **EAE** ($\lambda_{max}$ = 337 nm). This

comparative blue shift is attributed to the effective conjugation between only two of the three heterocycles in **EAE** (**Figure 4**). While the neutral spectra for each chromophore are unique, the radical cation spectra have surprisingly similar characteristics (energies and band widths). As predicted from **Figure 1**, there are two peaks in the radical cation spectra for each chromophore, the higher energy peak indicative of the singly occupied molecular orbital (SOMO) to LUMO transition (b) and the lower for SOMO-n to SOMO (c) (note only the high energy radical cation peak is shown in **Figure 3**). For the SOMO to LUMO transitions, there is only a 7 nm difference between the peak maxima of each chromophore. In the case of the lower energy transitions (refer to **Figure S2**), the peak maxima occur at 831 nm (**EPE**) and 809 nm (**EAE**) with similar oscillator strengths. These spectra demonstrate the ability to control the neutral state absorbance while producing nearly the same oxidized spectra. Thus, this theoretical experiment guides the focus of synthetic efforts towards highly strained acyclic systems to produce colorless neutral chromophores.

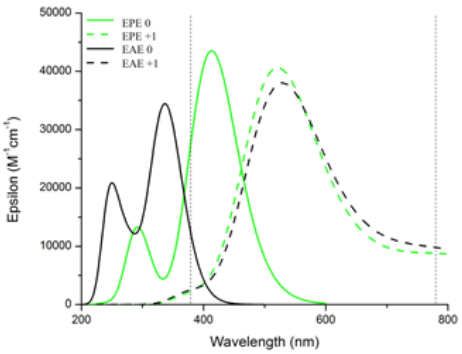


**Figure 3**: UV-Vis spectra of **EPE** and **EAE** in the neutral (solid) and radical cation (dashed) states. Vertical dotted lines indicate the visible range of 380-780 nm.

*III.2C Conjugation versus ring study:* We next focused our attention on designing materials that absorb little to no visible light in the neutral state, but exhibit broad absorbance upon oxidation. Through the incorporation of excess strain, the absorption of a chromophore is driven into the UV-region. Additionally, increasing the conjugation by utilizing more aromatic systems in a single chromophore facilitates the polaronic spectrum to absorb broadly in the visible. To this end, the methyl-capped four and five ring chromophores shown in **Scheme 2** were explored where the latter included dimethoxybenzene (**B**), which offers a high degree of strain and an inherently wider optical gap than thiophene-based systems due to an increased aromaticity. Apart from the dihedral angle data given in **Table 1**, we also analyzed the transitions which gave rise to those states with the highest oscillator strengths. Upon closer analysis of the frontier molecular orbitals (**Figure 4**), the majority of electron density in the ground-state is delocalized on the **EAB** portion of the chromophore; in essence half of the molecule. Due to the increased strain along the backbone, the effective conjugation along the chromophore is compromised, producing an optical gap comparable to that observed in **EAE**. It was determined based on this study as that EAE and EABAE were the most promising due to their high transmissivity coupled with their visible absorptions for both their neutral and radical cation states, respectively.

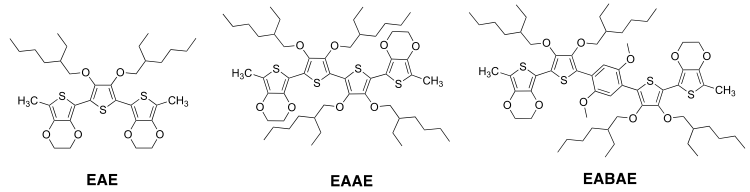


**Scheme 2**: Chromophores evaluated in the conjugation study.

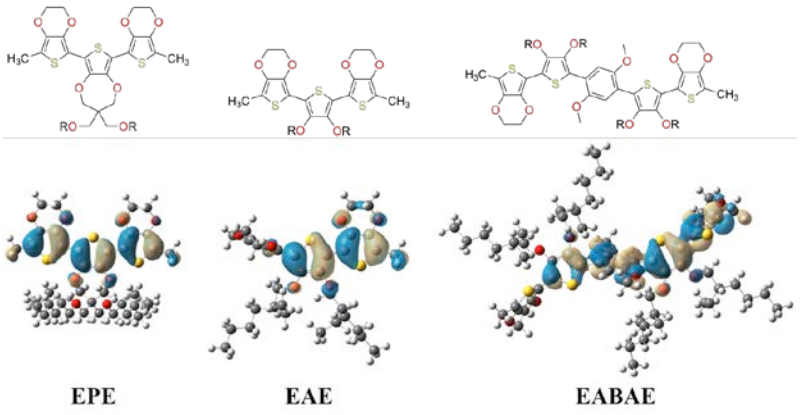


**Figure 4**: Frontier molecular orbital diagrams detailing the HOMO of the neutral, ground state energy of the three systems.

III.2D *Charge State Elucidation of pEABAE*: In the spectroelectrochemistry for **pEABAE** the charged state exhibited an unusually high-energy absorption characteristic compared to what was calculated. To elucidate the unusual charge state for this chromophore, computational methods were utilized. For this calculation, the chromophore is broken into pieces with the idea that the dimethoxybenzene would act as a steric block in the conjugation of the radical cation. **Figure 5** shows calculated radical cation state absorptions of segmented portions of the **EABAE** chromophore overlaid with the experimental spectroelectrochemistry. These calculations suggest that there are two main phenomena contributing to the radical cation spectra: twisted/conjugation broken chromophores and π-π stacking. As demonstrated by the frontier molecular orbitals in **Figure 4**, the computations strongly support that the two experimental peaks at 412 nm and 452 nm are contributions from the two-ring dioxythiophene portions of the chromophore (**EA**, 405 nm) and the three-ring fraction (**EAB**, 456 nm), respectively. Surprisingly, the results did not support any major influences from the full chromophore (**EABAE**, 496 nm). In an effort to identify the contributor(s) to the 587 nm peak, a radical cation π-dimer comprised of **EA** and **EAB** units was generated. This aggregate, producing a 562 nm peak, provides strong support that intermolecular π-π stacking is likely responsible for the low energy peak.[6, 8]

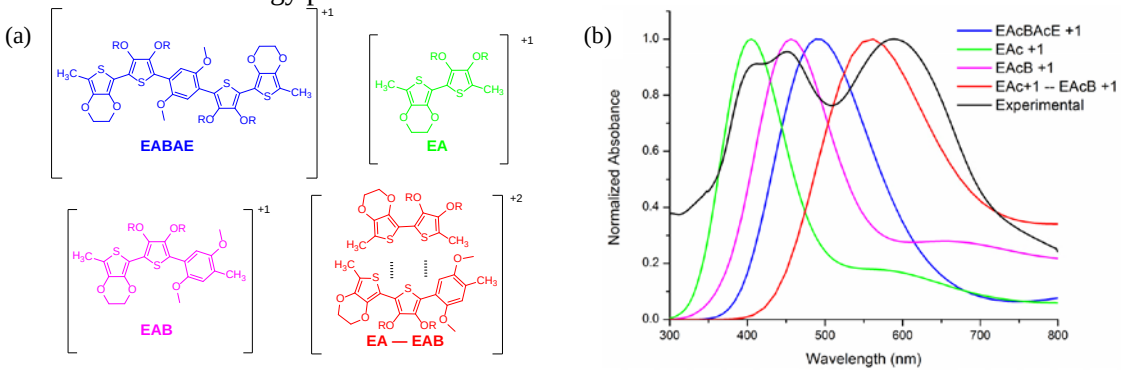


**Figure 5:** (a) Structures indicating where the steric blocks in the structure may occur for limiting the radical cation delocalization. These structures' absorptions were calculated to simulate a radical that is localized. **EA-EAB** is the π face interaction of the radical cation state of two portions of separate molecules (b) Calculated radical cation state absorptions of the segmented portions of the **EABAE** chromophore compared to the experimental data.

### *III.3 Ring Strain Stabilization Study*

*III.3A The Rationale and Setup for this Study:* Here, we examined the impact of the number, location and electron richness of substituted benzenes on a polymer's conformational and interring strain. **Figure 6** shows the set of oligomers used for this examination. A phenyl ring was sandwiched between two dioxythiophene rings terminated with methyl groups while the number, side-chain and type of substituent were varied. The use of alkyl groups allowed for modulation of the strain while maintaining similar electron donation into the pi system. Incorporation of amine and alkoxy substituents facilitated electron donation into the ring, while the strain was fined-tuned through the attached alkyl groups. In addition, we examined the HOMO and LUMO as well the interactions which occurred when S and O containing substituents were in close proximity to the S and O atoms in the adjacent aryl rings (S-S and O-O interactions were repulsive and S-O and O-S interactions were attractive). The examination of fluorine as a substituent provided a means for adding pi density to the chromophore while maintaining a relatively small, sterically compact atom (only about twice the atomic radius of a hydrogen).

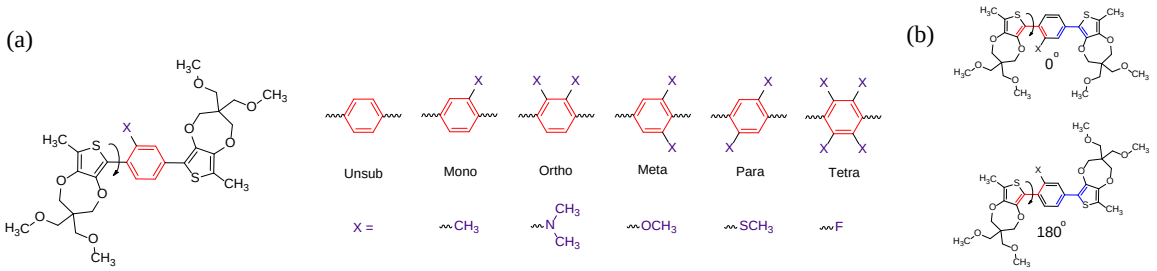


**Figure 6:** (a) Number, location and type of the substitution for the central benzene as well as the angle which will measured as these items are varied. (b) The definition of planarity for both the 0 and 180 degree angles.

For this study, we used the gold standard for DFT (functional B3LYP with 6-31G* basis set without solvent inclusion). For each substitution we began by optimizing the geometry. Next, the dihedral angle on the left was rotated (by 15 degrees) and frozen while the rest of the molecule was free during optimization. Finally, we took each of these outputs and applied TDDFT in order to generator optical band gap data. For all the studies we took differences between the energy or band gaps of optimized geometries and those for a given substitution pattern (or side-chain) constrained to the frozen angle.

*III.3B Instability of Ortho & Tetra Substitution Patterns:* We had quite a few issues with getting the ortho and tetra substitutions to converge. A closer examination revealed the issue where a curvature along the backbone is generated due to the extreme sterics caused by the tight proximity of forcing substituents into such a small space. This finding is evident in **Figure 7** where the ortho and tetra patterns are contrasted with the much less constricted mono version. For this reason these two designs were excluded from the remainder of the study.

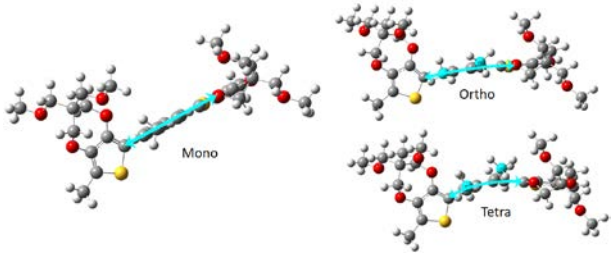


**Figure 7:** Comparison of Mono, Ortho and Tetra Substitution Patterns.

*III.3C Substitution Pattern Study:* We first examined the energetic barrier to rotation ($\Delta E = E_{Dihedral} - E_{Optimized}$) by plotting this energy difference versus the frozen dihedral angle for each substitution pattern (see **Figure 8**). For the unsubstituted case, the lowest energy was found to be both planar forms (dihedral angles 0° and 180°) with an energy maximum at 90°.

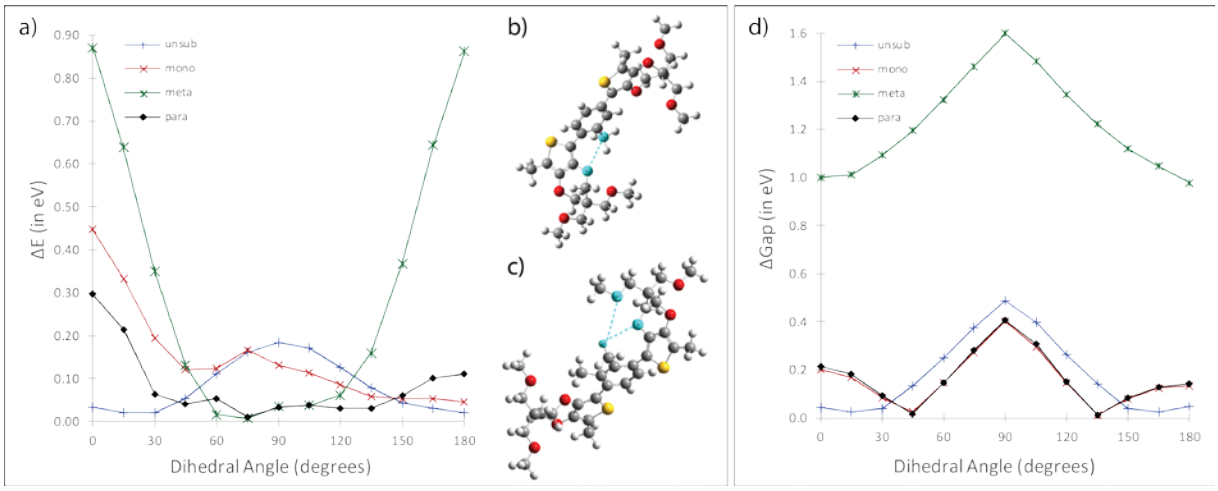


**Figure 8:** a) Energy versus dihedral angle plot for the four remaining substitution patterns. b) the interaction between the O-atom and the adjacent $CH_3$ group which produced the 75° maximum for the mono pattern. c) the stabilization which is produced from the interaction between the O-atom and the adjacent H-atoms leading to the 75° minimum. d) Difference in band gap values between the optimized and frozen geometry versus the corresponding dihedral angle.

The mono pattern had a minimum at 180° and maxima at 0° and 75° where the latter was due to the interaction between the O-atom and the adjacent $CH_3$ group as shown in **Figure 8 b)**. The meta pattern had a maxima at 0° and 180° with a minimum at 75° likely due to the stabilization between the O-atom and the two adjacent H-atoms (see **Figure 8 c**). Finally, the para pattern was quite similar to the meta with a minimum at 75° and maxima at 0° and 180°. From this study, we ascertained that meta and para substitution patterns provide the best stabilization of strain. We will capitalize on these patterns in our "Control of Radical Cations Study" discussed in the *Current and Future Research Efforts* section.

In adjacent study we examined how these substitution patterns impact the band gaps by plotting the band gap difference ($\Delta Gap = Gap_{Dihedral} - Gap_{Optimized}$) versus the frozen dihedral angle for each substitution pattern (see **Figure 8 d)**). All four patterns indicated a maximum difference at 90° which is not surprising as there is a clear break in conjugation at this angle. For the unsubstituted case, the lowest change in band gap was again found for the two planar forms which is consistent with the energy study. Both the mono and para patterns exhibited nearly identical patterns (the largest difference was 0.01 eV) with lowest gap difference occurring at 45° and 135° as well as an increase in the gap difference for the planar forms. The meta substitution pattern mirrored that for the unsubstituted but the overall gap difference was increased by 0.8 eV for all angles. We believe this is due to a steric effect which occurs on both side of the primary axis. Overall, we determined that the meta substitution pattern will provide the highest band gap change and as such would provide us with the means to ensure that oligomer/polymer will be blue-shifted into the UV.

*III.3D Side-Chain Study Using Mono Substitution Pattern:* In order to elucidate the impact of side-chain identity on the energy and band gap differences, each side-chain was placed into the mono substitution pattern and examined. **Figure 8 a)** shows the energy differences versus the dihedral angle. For all cases the highest energy difference occurred at 0°. For the remaining dihedral angles, there were two sets of side-chain patterns which emerged. The first set corresponding to $CH_3$ and $SCH_3$ demonstrated an increase at 180° and minima for $45° \leq \theta \leq 135°$ dihedral angles. The second set ($N(CH_3)_3$, $OCH_3$, and F) all demonstrated minima at 45° (local) and 180° (global). The local maximum was 75° for $N(CH_3)_3$ and 90° for both $OCH_3$ and F. All of these trends are believed to be due to stabilization or repulsive properties between the substituent with its adjacent neighbors. The impact of rotation on the change in band gap was found to be minimal with differences of 0.06 eV or less between all six side-chains for the 90° dihedral angle. The take home message for this study was that strain stabilization is best achieved with either alkyl or thioalkyl type side-chains.

### *III.4 All Donor Electrochromic Polymers*

Christiansen, D., Ohtani, S., Chujo, **Tomlinson, A.L.**, Reynolds, J.R. "All Donor Electrochromic Polymers Spanning the Visible Spectrum Through Random Copolymerization" *Chem. Mater.*, 31(17), 6841-6849, **Invited manuscript for a special issue honoring Jean-Luc Brédas,** DOI: 10.1021/acs.chemmater.9b01293

*III.4A The Rationale:* Here we used the CMY color mixing motif to form a plethora of chromophore units of differing absorbance in order to produce broad spectral coverage. For the cyan portion, we found a monomer which would produce a low energy absorbing material when combined with disubstituted 3,4-propylenedioxythiophenes (ProDOTs) into a copolymer. The magenta section was a ProDOT that will acted as a homo polymer which absorbs in the middle of the visible spectrum. Finally, for the yellow component, we found a monomer that may act as a high energy absorber when in a ProDOT copolymer.

*III.4B Generating a Library of Potential Absorbers*: A set of small oligomers was chosen to model possible random copolymers with varying degrees of conjugation and ring strain, as well as assess their influence on the predicted color. An examination of the calculated HOMO-LUMO gaps provided direction with respect to the potential spectral breath, or the absorption tunability limits which may be attained by the copolymers. As the strain along the backbone was increased by adding DAT units, the HOMO-LUMO

gap widened. Oligomers possessing the most DAT rings were particularly influenced by distortion from planarity causing a band gap increase. The most twisted species (most deviated from the defined 180° trans planar geometry) were **DPPD**, **DPDP**, **DEED** and **DPDPDP** with values as low as 128.3°, 156.9°, 136.9° and 46.8°, and corresponding band gaps of 3.09 eV, 2.98 eV, 2,72 eV, and 2.53 eV, respectively (see **Table 3**). **DPDPDP** was the only 6-aryl group oligomer to be greatly impacted by inclusion of DAT as compared to **PDEEDP** which possesses a band gap that is nearly 0.2 eV smaller. The remaining oligomers demonstrated that conjugation extension reduced the band gap as seen in **EEPPEE** and **PEEPEE**.

**Table 3**. Band gaps, dihedral angles and visible excited state wavelengths and oscillator strengths for the target oligomers. The legend indicates how the structures and their corresponding dihedral angles are defined.


| Oligomer | $E_g$ (eV) | Dihedral Angles | | | | | Peak Maximum | |
|---|---|---|---|---|---|---|---|---|
| | | Ar1-Ar2 | Ar2-Ar3 | Ar3-Ar4 | Ar4-Ar5 | Ar5-Ar6 | λ (nm) | *f* |
| **PEEP** | 2.62 | 179.7 | 178.1 | 179.7 | | | 473.3 | 1.6005 |
| **EEPEE** | 2.38 | 176.4 | 178.7 | 178.7 | 176.4 | | 521.1 | 2.0269 |
| **PEEPEE** | 2.22 | 179.3 | 177.9 | 179.0 | 179.7 | 178.5 | 559.6 | 2.4779 |
| **DEED** | 2.72 | 156.9 | 179.7 | 156.9 | | | 456.6 | 1.5363 |
| **EEDEE** | 2.45 | 178.3 | 168.4 | 168.4 | 178.3 | | 506.4 | 1.9432 |
| **EEPPEE** | 2.23 | 178.4 | 179.2 | 175.9 | 179.2 | 178.4 | 556.7 | 2.4360 |
| **DPPD** | 3.09 | 46.8 | 175.6 | 48.9 | | | 401.3 | 1.2749 |
| **PDPDP** | 2.49 | 169.1 | 176.9 | 176.9 | 169.1 | | 497.4 | 1.7931 |
| **PDEEDP** | 2.35 | 163.7 | 163.0 | 179.6 | 163.0 | 163.7 | 528.6 | 2.2510 |
| **DPDP** | 2.98 | 137.2 | 160.9 | 136.9 | | | 416.2 | 1.1896 |
| **DPDPD** | 2.48 | 178.6 | 179.9 | 179.9 | 178.6 | | 500.8 | 1.9028 |
| **DPDPDP** | 2.53 | 166.2 | 179.1 | 178.2 | 169.9 | 128.3 | 489.9 | 2.5072 |

The calculated UV-Vis spectra of these systems provided visible peak maxima that varied from 401 nm to 560 nm, spanning a difference of nearly 160 nm. Of the 15 generated excited states, only 3 or 4 possessed oscillator strengths of 0.1 or higher. Aside from the peak maxima location there are no differences in the predicted peak shapes in the visible range (**Figure 9**). In fact, the set of oligomers possessing 5 aryl groups produce nearly identical spectra and have peak maxima which differ by only 24 nm. The 4 and 6 aryl group structures are more impacted by torsion along the backbone and had ranges of 72 nm and 70 nm, respectively.

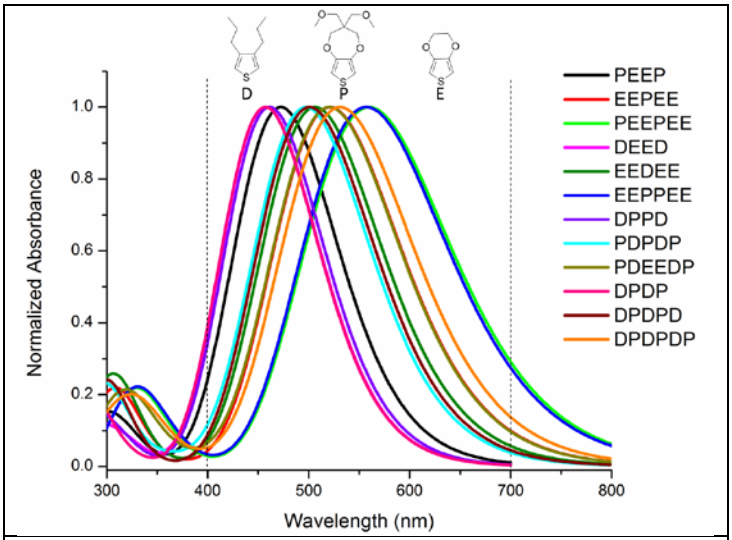


**Figure 9**. The calculated absorbance of the model chromophores with truncated side chains

The simulated UV-Vis of these molecules also provided a means to estimate the color which may be produced in the CIE L*a*b* color space.[19–21] Positive a*and b* values represent red and yellow while the negative values indicate blue and green, respectively. As the magnitudes of a* and b* increase, the color becomes more saturated, and as one traverses between color points, the hue changes. L* depicts the lightness: a value of 0 would be black and 100 would be white. The L*, a*, and b* coordinates were translated to the RGB color space in order to predict the oligomeric color. **Figure 10** shows the results of this prediction along with the corresponding HOMO, LUMO and first excited state band gap values for each system. The predicted colors give a range of the color space that could be reached and matched well to what was achieved experimentally.

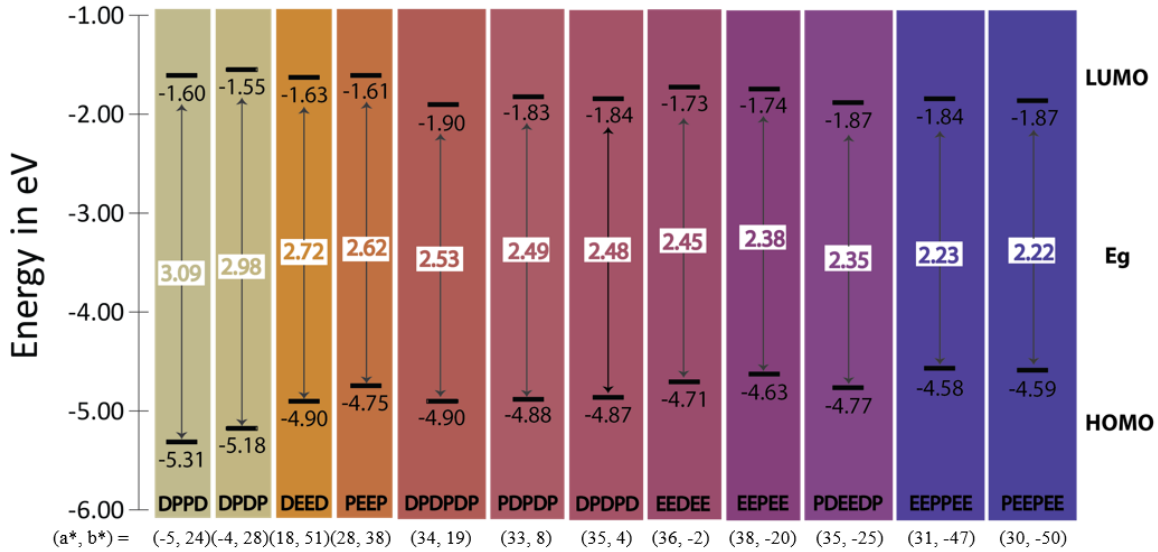


**Figure 10:** Oligomers are arranged in order of decreasing first excited state band gap. The corresponding HOMO, LUMO and RGB color are provided. The corresponding (a*, b*) values are given below the corresponding energy level diagram.

### *III.5 Color Control of Radical Cations*

*III.5A The Hypothesis:* If electron rich or poor moieties in the meta position can be used to increase or decrease the energy of the SOMO then we can control where the charged state will absorb. In other words, we can tune the substitution pattern in order to produce radical cations which absorb across the visible spectrum. The types of electronic transitions which occur upon absorption for radical cations is shown in **Figure 11**. As indicated on the left, when there is a lack of electron density the difference between the SOMO level and that of SOMO-1 and LUMO is larger leading to absorption peaks a and b. There is a reduction in this difference when an electron rich moiety is involved (right side of **Figure 11)** leading to absorption peaks c and d.

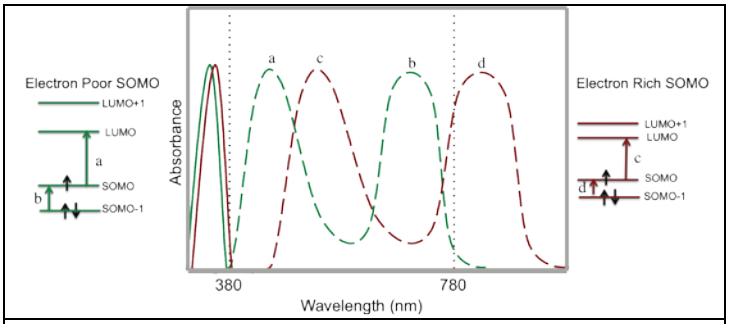


**Figure 11:** Impact on electron richness of moiety on the SOMO level which leads to differences in absorption pattern.

*III.5B Meta Position Control*: In order to guide experiment and probe the design paradigm from a molecular orbital perspective, time dependent density functional theory (TDDFT) calculations were performed on these molecules and theoretical spectra were generated for the neutral and radical cation states of the molecules (see **Figure 12)**. As can be seen in comparing the solid curves, there is minimal change in the absorbance of the neutral molecules upon the addition of electron rich moieties at the *meta*-position. All of the spectra have a $\lambda_{max}$ in the UV with absorption onsets ~400 nm. However, when examining the radical cation spectra there are stark differences. While the high-energy absorption appears to be consistent between these molecules, there is a significant alteration in energies between the long wavelength transitions as evidenced by a red-shifting of this peak. There is a particularly large red-shift going from **ACE2** to **ACE3**, upon addition of a methoxy group to the *meta*-position, which is consistent with the energy levels, oscillator strengths, and frontier molecular orbitals (FMOs).

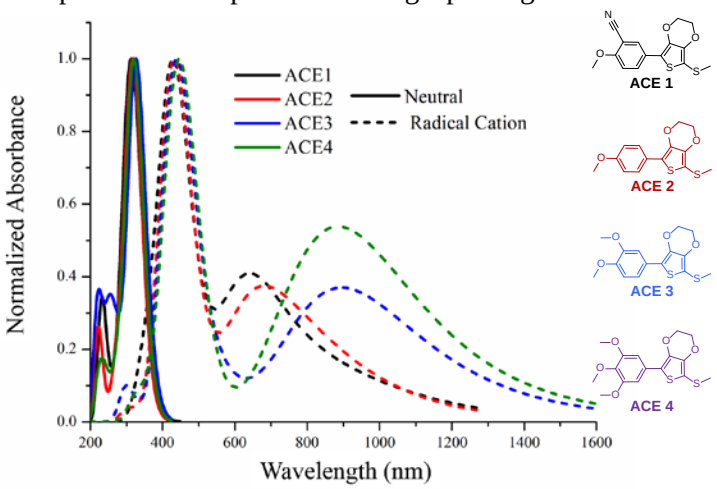


**Figure 12:** TDDFT calculated spectra for the neutral and radical cation states for the molecules in this study.

A detailed analysis of the TDDFT oscillator strengths provides some insight into the absorption differences for these radical cations, **Table 4**. In all cases, the transition which carries the largest oscillator strength (*f*) is the SOMOα→LUMOα (Sα→Lα) which remains relatively unchanged (434-435 nm) until **ACE4** (449 nm). It is the remaining significant transitions (those possessing $f \geq 0.1$) which are believed to control the color. For **ACE1**, there was a transition found for the SOMO-1β→LUMOβ (S-1β→Lβ) corresponding to 636 nm. In the case of **ACE2**, the Sβ−1→Lβ transition was slightly red-shifted to 650 nm and the appearance of a SOMOβ→LUMOβ (Sβ→Lβ) at 846 nm was produced. The oscillator strength for the Sβ→Lβ transition for **ACE3** increases relative to the S-1β→Lβ transition and red-shifts to 863 nm. Finally, **ACE4** indicated the largest red-shift for the Sβ→Lβ transition at 900 nm and further decrease in the oscillator strength associated with the S-1β→Lβ transition. Interestingly, **ACE4** has a second high-energy transition of significant oscillator strength in the visible at 406 nm associated with the S-3β→Lβ transition.

**Table 4.** Oscillator Strengths and Transitions of Radical Cations

| Molecule | λ (nm) | f | Dominant Transition |
|---|---|---|---|
| **ACE1** | 636 | 0.24 | S-1β→Lβ |
| **ACE1** | 435 | 0.52 | Sα→Lα |
| **ACE2** | 847 | 0.10 | Sβ→Lβ |
| **ACE2** | 650 | 0.22 | S-1β→Lβ |
| **ACE2** | 434 | 0.63 | Sα→Lα |
| **ACE3** | 863 | 0.13 | Sβ→Lβ |
| **ACE3** | 690 | 0.15 | S-1β→Lβ |
| **ACE3** | 434 | 0.63 | Sα→Lα |
| **ACE4** | 900 | 0.28 | Sβ→Lβ |
| **ACE4** | 449 | 0.50 | Sα→Lα |
| **ACE4** | 406 | 0.14 | Sβ-3→Lβ |

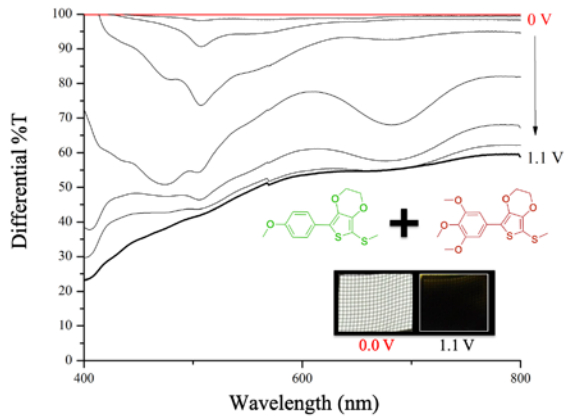


**Figure 13:** Differential spectroelectrochemistry performed with an OTTLE of a 1:1 mixture of **ACE2** and **ACE4** with photographs in the inset at the extreme potentials as noted.

A 1:1 mixture of **ACE2** and **ACE4** was created and the differential spectroelectrochemistry and photography is detailed in **Figure 13**. As can be seen from the photography, the mixture changes from a color neutral, transmissive solution to an opaque black. One can imagine that the blends can be adjusted to create browns and other secondary colors from only a few molecules, as the library of ACE molecules is expanded.

Quantum chemical calculations give insight into how energy levels are manipulated to control transition dominance in odd-electron systems and guide molecular design to create new anodically coloring electrochromic molecules. It has been shown that these molecules have overcome the contrast barrier present in the field of organic electrochromism while maintaining a wide variety of tunable colors and secondary blends.

*I11.5C Para Position Control*: For this set we wanted to determine how changes at the para position would impact radical and neutral coloration. To this end we applied our DFT model to **ACE5-ACE8** and performed a detailed excited state transition analysis which produced our simulated UV-Vis spectra (see **Figure 14**). Unlike the **ACE1-ACE4**, there are differences in the neutral spectra. However, the radical cation for this set did mimic the meta systems where higher energy possessed the largest oscillator strength and was a consequence of the $S_\alpha \rightarrow L_\alpha$ with a range of. 420 nm to 448 nm. The remaining absorptions are the majority of the color generation origin. As the electron donation was increased the peak maximum for the lower energy peak was red-shifted. In the case of **ACE5-ACE7** this peak was partly due to $S_\beta\text{-}1 \rightarrow L_\beta$. For both **ACE7** and **ACE8** the absorption peak was the result of a transition from $S_\beta \rightarrow L_\beta$. Overall these results support a means to further expand the ACE color palette.

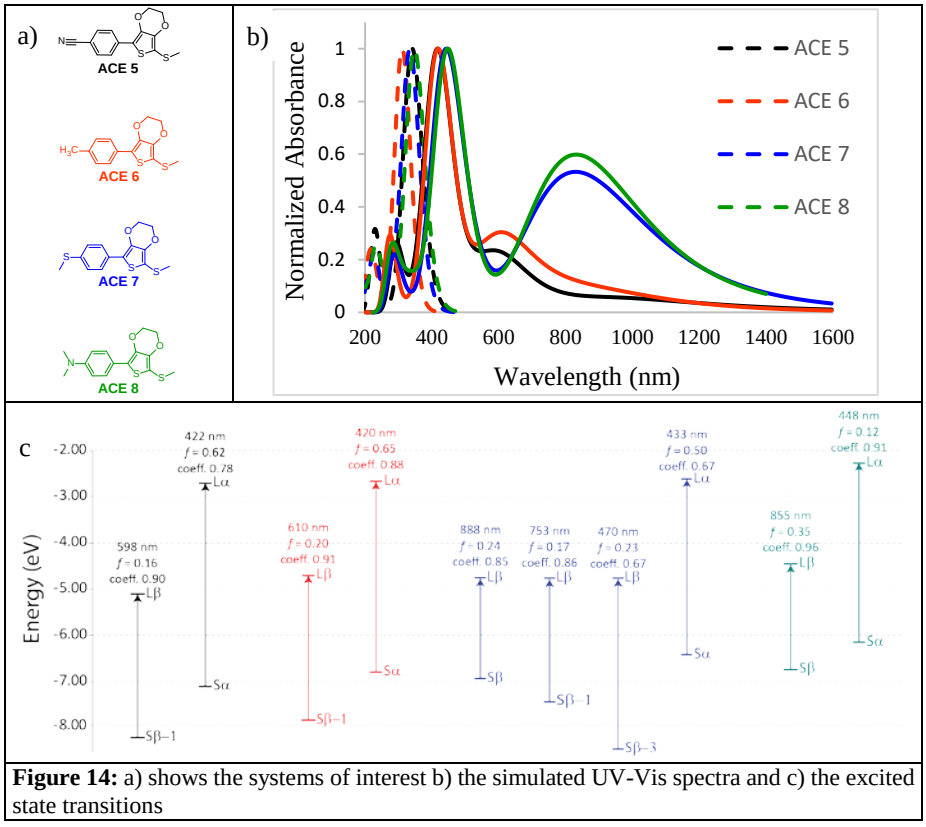


**Figure 14:** a) shows the systems of interest b) the simulated UV-Vis spectra and c) the excited state transitions

### *III.6 Symmetric and Asymmetric Systems*

*III.6A The Hypothesis:* We can use symmetry selection rules to limit the number of allowed photoexcited transitions which will then provide control of the shape of the absorbance peak (both width and intensity). **Figure 15** demonstrates the hypothesis using a) an example set of systems, b) the allowable radical cation excited state transitions and c) the resulting UV-Vis spectra. For symmetric systems the electronic transitions between states with the same symmetry are forbidden (e.g. $SOMO_{\beta}$-1→ $LUMO_{\beta}$). As there are less allowable excited states the result will be a sharper higher energy peak than the asymmetric ACE. Additionally, the induction of asymmetry should push the lower energy peak further into the NIR.

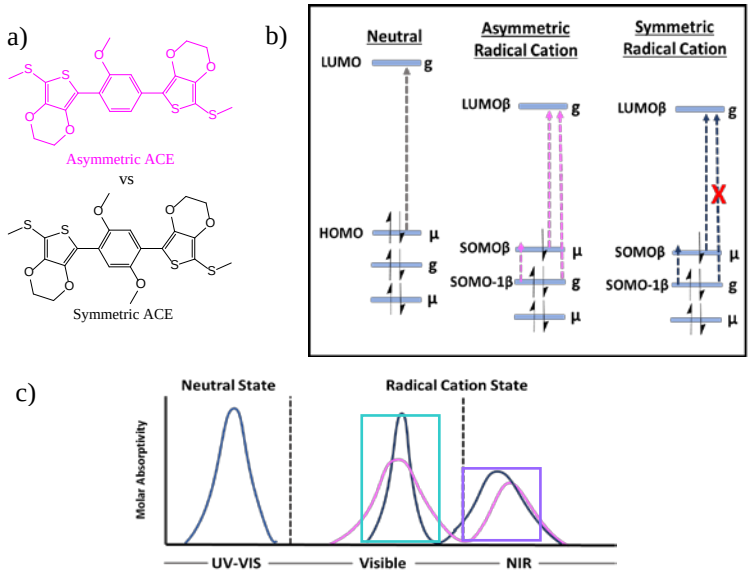


**Figure 15:** a) Example asymmetric and symmetric systems, b) allowable transitions, and c) resulting UV-Vis

For our systems of interest, we sandwich a benzene varying methoxy substituents between two EDOTs (**Figure 16**). The neutral simulated UV-Vis spectra and optimized geometries demonstrated the spectra for the **ASYM1** and **SYM2** pair, the **ASYM2** and **ASYM3** pair and the **ASYM4** and **SYM1** pair had very similar excited absorption maxima as well as dihedrals as shown in **Figure 17**. A comparison between **ASYM2, ASYM3**, and **SYM1** who all possessed 2 methoxy groups indicated that the more symmetric a system is the less it is strained. An examination of the radical cation spectra revealed a continuation of the pairings between the 6 systems. For the lower energy peaks the range for the absorption peak maxima was between 1059 – 1455 nm. In **Figure 18**, we have a close look at visible absorption spectra (ranging from 380 – 780 nm) as well as the excited state transitions from which these peaks arose (**Figure 19**). In case of **ASYM1** and **SYM2**, there was a difference of 5 nm between the peak maxima and the primary transition generated from the $SOMO_{\alpha}$-1→ $LUMO_{\alpha}$. Also, **ASYM1** had an additional transition which gives some credence to idea that there are more allowable transitions for asymmetric systems. The **ASYM2** and **ASYM3** pair had 3 excited states where the $SOMO_{\alpha}$→ $LUMO_{\alpha}$ (difference of 21 nm) possessed the highest oscillator strength for both. This pair also had the $SOMO_{\beta}$→ $LUMO_{\beta}$+1 (difference of 18 nm) transition in common. For

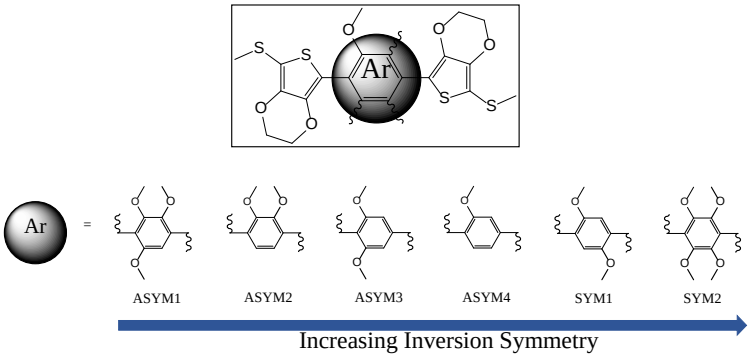


**Figure 16**: Systems of interest for symmetry/asymmetry study

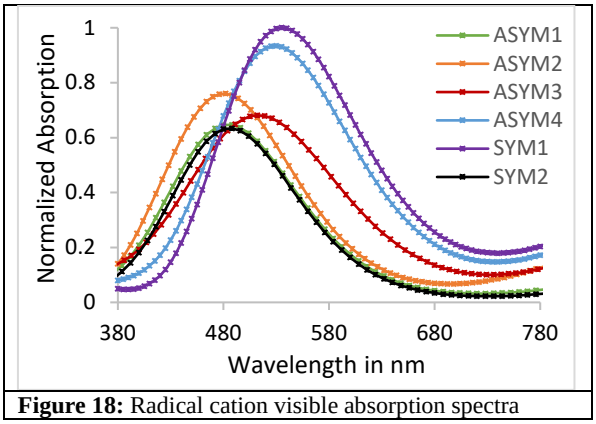


**Figure 18:** Radical cation visible absorption spectra

**ASYM4** and **SYM1** both had 1 allowable excited state transition which doesn't follow our hypothesis (**ASYM 4** would be expected to possess more than 1). Furthermore, both of these ACEs had the largest oscillator strength which again is contrary to our supposition that symmetry will lead to a sharper peak morphology. Additionally, there was the only a 5 nm difference between their peak maxima ($SOMO_\alpha \rightarrow LUMO_\alpha$) which contradicts our statement that more asymmetry should result in red-shifted lower energy peaks. Overall we learned that while symmetry may be able to tell us the number of anticipated transitions it is dihedral angle strain which dictates the location, sharpness of the peaks and therefore the color for the system.

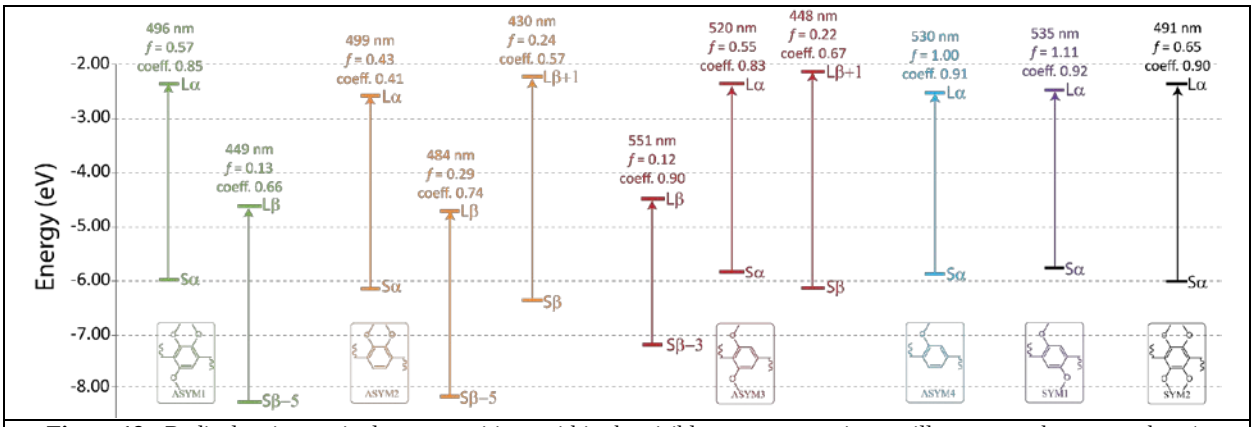


**Figure 19:** Radical cation **e**xcited state transitions within the visible range possessing oscillator strengths greater than 1.

## IV. Personnel Supported with salary:

Principal Investigator:

Aimée Tomlinson

Undergraduate Students:

Lily Rainwater Diodati
Melody Mullen
Alex Diodati
Aaron Morrenzin

## V. References


1. Frisch, M. J. T., G. W.; Schlegel, H. B.; Scuseria, G. E.; Robb, M. A.; Cheeseman, J. R.; Scalmani, G.; Barone, V.; Mennucci, B.; Petersson, G. A.; Nakatsuji, H.; Caricato, M.; Li, X.; Hratchian, H. P.; Izmaylov, A. F.; Bloino, J.; Zheng, G.; Sonnenberg, J. L.; Hada, M.; Ehara, M.; Toyota, K.; Fukuda, R.; Hasegawa, J.; Ishida, M.; Nakajima, T.; Honda, Y.; Kitao, O.; Nakai, H.; Vreven, T.; Montgomery, Jr., J. A.; Peralta, J. E.; Ogliaro, F.; Bearpark, M.; Heyd, J. J.; Brothers, E.; Kudin, K. N.; Staroverov, V. N.; Kobayashi, R.; Normand, J.; Raghavachari, K.; Rendell, A.; Burant, J. C.; Iyengar, S. S.; Tomasi, J.; Cossi, M.; Rega, N.; Millam, N. J.; Klene, M.; Knox, J. E.; Cross, J. B.; Bakken, V.; Adamo, C.; Jaramillo, J.; Gomperts, R.; Stratmann, R. E.; Yazyev, O.; Austin, A. J.; Cammi, R.; Pomelli, C.; Ochterski, J. W.; Martin, R. L.; Morokuma, K.; Zakrzewski, V. G.; Voth, G. A.; Salvador, P.; Dannenberg, J. J.; Dapprich, S.; Daniels, A. D.; Farkas, Ö.; Foresman, J. B.; Ortiz, J. V.; Cioslowski, J.; Fox, D. J *Gaussian 09, Revision A.1*, Gaussian, Inc.: : Wallingford, CT, , 2009.
2. Barone, V.; Cossi, M., Quantum calculation of molecular energies and energy gradients in solution by a conductor solvent model. *J. Phys. Chem. A* **1998,** *102*, 1995-2001.

3. Cossi, M.; Rega, N.; Scalmani, G.; Barone, V., Energies, structures, and electronic properties of molecules in solution with the C-PCM solvation model. *J. Comp. Chem.* **2003,** *24*, 669-681.
4. Ferdous, S.; Lagowski, J. B., Comparison of ground and excited state polarizabilities of thiophene, cyclopentadiene, and fulvene oligomers and their cyano substituted derivatives—Ab initio study. *Journal of Polymer Science Part B: Polymer Physics* **2007,** *45* (15), 1983-1995.
5. Jacquemin, D.; Adamo, C., Bond Length Alternation of Conjugated Oligomers: Wave Function and DFT Benchmarks. *Journal of Chemical Theory and Computation* **2010,** *7* (2), 369-376.
6. McCormick, T. M.; Bridges, C. R.; Carrera, E. I.; DiCarmine, P. M.; Gibson, G. L.; Hollinger, J.; Kozycz, L. M.; Seferos, D. S., Conjugated Polymers: Evaluating DFT Methods for More Accurate Orbital Energy Modeling. *Macromolecules* **2013,** *46* (10), 3879-3886.
7. Wang, E.; Ma, Z.; Zhang, Z.; Vandewal, K.; Henriksson, P.; Inganäs, O.; Zhang, F.; Andersson, M. R., An Easily Accessible Isoindigo-Based Polymer for High-Performance Polymer Solar Cells. *Journal of the American Chemical Society* **2011,** *133* (36), 14244-14247.
8. Scherlis, D. A.; Marzari, N., π-Stacking in Charged Thiophene Oligomers. *The Journal of Physical Chemistry B* **2004,** *108* (46), 17791-17795.